Check for updates

doi.org/10.1002/hlca.202100221

RESEARCH ARTICLE

HELVETICA chimica acta

Circularly Polarized Luminescence of [6]Helicenes through Excited-State Intramolecular Proton Transfer

Dominik Göbel[+],[a] Sandra Míguez-Lago[+],[b] Maria Jose Ruedas-Rama,[c] Angel Orte,[c] Araceli G. Campaña,*[b] and Michal Juríček*[a]

[a] Department of Chemistry, University of Zurich, Winterthurerstrasse 190, CH-8057 Zurich, Switzerland, e-mail: michal.juricek@chem.uzh.ch; michal.juricek@gmail.com

[b] Department of Organic Chemistry, Chemistry Excellence Unit (UEQ), Faculty of Chemistry, University of Granada, ES-18071 Granada, Spain, e-mail: araceligc@ugr.es

[c] Nanoscopy-UGR Laboratory, Department of Physical Chemistry, Faculty of Pharmacy, Chemistry Excellence Unit (UEQ), University of Granada, ES-18071 Granada, Spain

Dedicated to *Peter Kündig* on the occasion of his 75th birthday

© 2022 The Authors. Helvetica Chimica Acta published by Wiley-VHCA AG. This is an open access article under the terms of the Creative Commons Attribution Non-Commercial NoDerivs License, which permits use and distribution in any medium, provided the original work is properly cited, the use is non-commercial and no modifications or adaptations are made.

We present the concept of combining circularly polarized luminescence (CPL) and excited-state intramolecular proton transfer (ESIPT) features into a single molecule as a strategy to generate high-performance ESIPT-based CPL materials. For this purpose, a [6]helicene bearing two ESIPT structural units was synthesized using a double *Suzuki–Miyaura* reaction and a double C(sp^2)–H hydroxylation approach. The photophysical properties of the doubly hydroxylated [6]helicene were studied in parallel with a non-hydroxylated [6]helicene control compound, revealing that the presence of a chiral [6]helicene unit results in a strong CPL response and the presence of the ESIPT units in a considerable red shift. The red-shifted emission along with the outstanding g_{lum} ($\approx 10^{-2}$) and a large *Stokes* shift makes the doubly hydroxylated [6]helicene a promising candidate for use in optoelectronics.

Keywords: chirality, circularly polarized luminescence, excited-state intramolecular proton transfer, helicene, luminescence, proton transfer.

Introduction

Artificial lighting and light-triggered technologies play an important role in modern society and the current trend suggests that their significance will continue to increase. While common luminescent materials generate unpolarized light, the current focus is on materials that generate circularly polarized (CP) light, encoding chirality as an additional information channel. Since the CP light acts as an intrinsic chiral information carrier, materials that produce CP light hold potential for applications in light-emitting devices,[1–3] biological probes,[4,5] and CP-light lasers.[6] The chemical approach to obtain CP light is the design of chiral luminescent materials, which display circularly polarized luminescence (CPL),[7–9] whose efficiency is evaluated by the luminescence dissymmetry factor (g_{lum}).[1]

[+] These authors contributed equally to this work.

Supporting information for this article is available on the WWW under https://doi.org/10.1002/hlca.202100221

[1] g_{lum} is defined as $g_{lum} = 2 \times [(I_L - I_R)/(I_L + I_R)]$, where I_L and I_R are the intensities of left- and right-handed polarized light, respectively. The g_{lum} values range from -2 to $+2$ with negative values for the right-handed and positive values for the left-handed light. A value of 0 indicates unpolarized light and a value of $|2|$ completely circularly polarized light.

The exploration of chiral organic small molecules that exhibit CPL, like helicenes, is of particular interest, due to the easiness of modulating their emission features through structural design.[10–13] Helicenes are *ortho*-fused polyaromatic structures with a twisted shape resulting from the steric repulsion between the terminal aromatic rings.[14,15] Consequently, they adopt left- or right-handed helical geometries and exhibit in many cases efficient CPL emission.[10–13] Since the first report of CPL-active helicenes in 1966,[16] a variety of carbo-, hetero-, and metal helicene analogs that display CPL were synthesized and characterized.[10,17]

The judicious incorporation of substituents into a carbohelicene scaffold was found to modulate their photophysical properties and afford a new generation of systems with improved CPL. For example, the incorporation of a quinoline unit into [7]helicene conducted by *Sakai et al.*[18] yielded a fully aromatic structure exhibiting small Φ_F that was significantly increased upon alkylation to afford (*M*/*P*)-**1** with Φ_F of 25% and $|g_{lum}|$ of 4.0×10^{-3} (*Scheme 1,a*). By integrating a fluorene fragment into the helicene framework, a large increase of emission efficiency was observed. Whereas [7]helicene exhibits a poor Φ_F of 2%,[19] (*M*/*P*)-**2** showed intense emission with a quantum efficiency up to 40% (*Scheme 1,b*).[20] Moreover, as a purely carbon-based helicene, (*M*/*P*)-**2** exhibits a relatively high $|g_{lum}|$ value of 3.0×10^{-3}. Privileged architectures, such as exciton-coupled systems, result in g_{lum} values in the range of 10^{-2}. *Crassous et al.* reported a variety of push–pull helicenes difunctionalized at the extremities of the carbo[6]helicene moiety (positions 2 and 15), in which the magnitude and the optimized mutual orientation of the electric (μ_e) and magnetic (μ_m) transition dipole moments in the excited state lead to an intense exciton-coupling

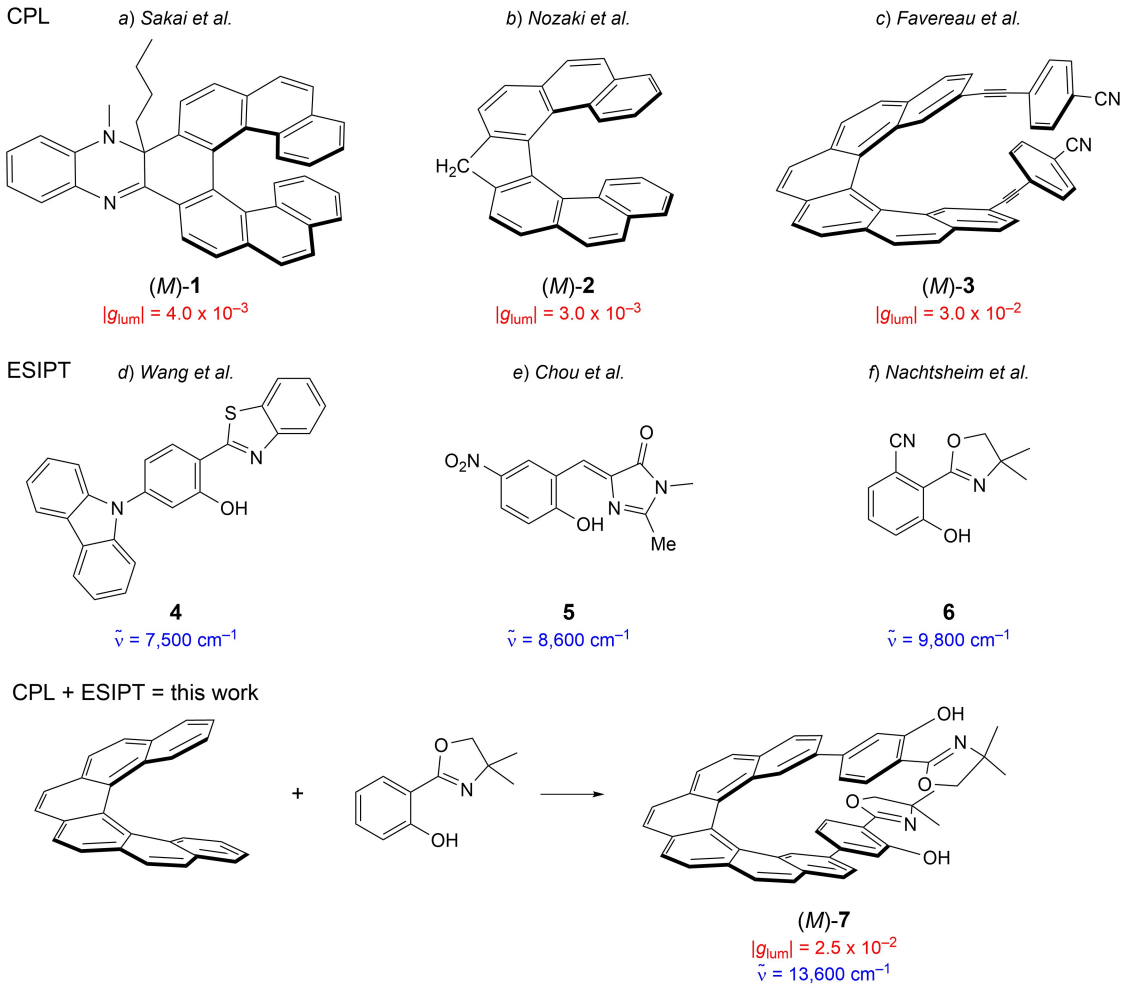

Scheme 1. Examples of CPL-active helicenes (top) and ESIPT-active luminophores with high *Stokes* shifts (middle). Bottom: The concept of combining a CPL unit with an ESIPT unit developed in this work (**7** was analyzed in CH_2Cl_2).

 © 2022 The Authors. Helvetica Chimica Acta Published by Wiley-VHCA AG

process.[21–25] The attachment of electron-poor, as in cyano-substituted luminophore (*M*/*P*)-**3** (*Scheme 1,c*), and electron-rich phenyl groups via acetylene spacer resulted in $|g_{lum}|$ values of up to 3.0×10^{-2}.[21]

A major disadvantage of most fluorophores is that they exhibit small *Stokes* shifts, which leads to self-reabsorption of the emitted light in concentrated media due to the overlap of the absorption and emission spectra. Excited-state intramolecular proton transfer (ESIPT)-based fluorophores operate in a four-level enol–keto-phototautomerism cycle (see *Scheme S1*), which results in large *Stokes* shifts of the emission (up to 12,000 cm^{-1}) without the tendency of self-reabsorption.[26–28] Within this cycle, upon enol excitation, an ultrafast[29] phototautomerism and emission of the keto form takes place followed by a ground-state intramolecular proton transfer (GSIPT). In the case of an incomplete proton transfer in the excited state, dual emission[30] properties can be observed. Furthermore, a wide range of ESIPT applications, for example, in electroluminescent devices,[28,31–33] biological imaging,[34–37] and chemical sensing,[26,38,39] have been demonstrated.

ESIPT-based luminophores exhibiting high *Stokes* shifts and high quantum yields are, however, still rare. A representative example reported by *Wang et al.* is 2-(2′-hydroxyphenyl)benzothiazole (**4**) showing an extremely high quantum yield of 91.7% in the solid state and a high *Stokes* shift of 7,500 cm^{-1} (*Scheme 1,d*).[33] Besides, *ortho*-hydroxy derivatives of the green fluorescent protein chromophore were investigated by *Chou* and coworkers.[40] Varying the donor/acceptor ability of the substituent on the central benzene ring resulted in emission-color tuning and quantum yields of up to 57% in the CH_2Cl_2 solution for the nitro-derivate **5** and an emission with a *Stokes* shift of 8,600 cm^{-1} (*Scheme 1,e*). In addition, a series of minimalistic ESIPT-based luminophores differing in their substitution pattern of electron-withdrawing and -donating groups were presented by *Nachtsheim et al.*[41,42] From all investigated regioisomers, nitrile-substituted 2-(oxazolinyl)phenol **6** exhibited the highest quantum yield of 87.3% in the solid state, while a moderate value of 25% was obtained in the CH_2Cl_2 solution with a high *Stokes* shift of 9,800 cm^{-1} (*Scheme 1,f*).

While both phenomena – CPL and ESIPT – were studied in great detail on a variety of aromatic systems independently of one other, the combination of both effects within a single molecule has never been described. Structures that would exhibit both CPL and ESIPT would benefit from the combination of both phenomena in terms of quantum efficiency and large *Stokes* shifts of CPL. To establish this concept, we report a [6]helicene emitter equipped with two ESIPT units. The synthetic strategy as well as a comprehensive analysis of the photophysical properties is presented for the doubly hydroxylated compound **7** as well as for the non-hydroxylated control compound **8**.

Results and Discussion

The synthesis of the target dihydroxylated helicene **7** was achieved in five steps starting from 2,7-dibromonaphthalene (*Scheme 2*).

Metal–halogen exchange using 2,7-dibromonaphthalene and ^{t}BuLi followed by formylation of the intermediate dilithio species with DMF provided dicarbaldehyde **9** in 82% yield. A *Wittig* olefination of **9** with phosphonium bromide **10** afforded a mixture of (*E*/*Z*)-isomers of olefin **11** in 84% yield. Next, *Mallory* photoinduced cyclization of **11** to dibrominated [6]helicene **12** was achieved under dilute conditions in the presence of iodine and propylene oxide with an average yield of 97%.[43] With dibrominated [6]helicene **12** in hand, a double *Suzuki–Miyaura* reaction with borylated 2-(phenyl)oxazoline **13** was performed to give doubly arylated [6]helicene **8** in a 51% yield. In the final step, the two hydroxy groups were installed in the benzene units *ortho* to the oxazoline rings using metalation with *Knochel–Hauser* base TMPMgCl·LiCl followed by oxidation with molecular oxygen to the corresponding diphenol **7** obtained as a racemic mixture.

With target helicenes **7** and **8** in hand, we investigated the photophysical properties of their racemic mixtures. The UV-Vis absorption spectra of **7** and **8** measured in CH_2Cl_2 show intense $\pi-\pi^*$ absorption bands at 270 and 295 nm, as well as shoulders at around 337 nm, with molar extinction coefficients for the higher-intensity bands of 51,000 $M^{-1}cm^{-1}$ (**7**) and 70,000 $M^{-1}cm^{-1}$ (**8**) at 270 and 295 nm, respectively. Compound **7** dissolved in CH_2Cl_2 shows an emission band with a vibronic structure peaking at 426 and 453 nm, and a broad shoulder from 500 to 600 nm (*Figure 1,a*). In contrast, compound **8**, in which ESIPT is not plausible, shows solely a band with a clear vibronic structure in both solvents (*Figure 1b*), equivalent to the blue-shifted band of compound **7**. The detected emission maxima imply large *Stokes* shifts of *ca.* 13,600 and 10,400 cm^{-1} for compounds **7** and **8**, respectively (*Figure 1a,b*). The fluorescence quantum yields (Φ_F) of 8.8% (**7**) and

 © 2022 The Authors. Helvetica Chimica Acta Published by Wiley-VHCA AG

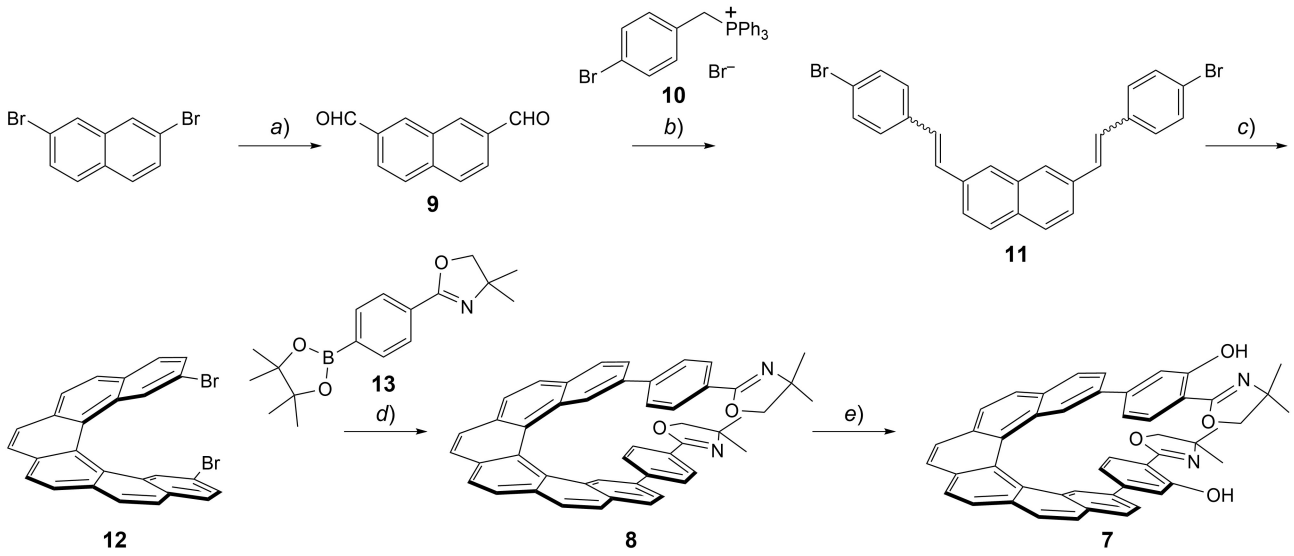

Scheme 2. Synthesis of the target dihydroxylated helicene **7**. Reaction conditions: *a*) 1. ^{t}BuLi, THF, −78 °C, 0.5 h; 2. DMF, −78 °C to 23 °C, 18 h, 82 %. *b*) **10**, KO^{t}Bu, THF, 23 °C, 16 h, 84 %. *c*) I_2, propylene oxide, hν, PhMe, 23 °C, 1.5 h; 97 % (combination of six runs). *d*) **13**, $Pd(PPh_3)_4$, SPhos, K_2CO_3, 1,4-dioxane:water 5:1 (v/v), 100 °C, 48 h, 51 %. *e*) *1*) TMPMgCl·LiCl, THF, 23 °C, 4 h; 2. O_2 (1 atm), 23 °C, 48 h, 51 %. Ph = phenyl, TMP = 2,2,6,6-tetramethylpiperidinyl.

8.7 % (**8**) represent a 2.2-fold increase of emission intensity in comparison to the parent [6]helicene (Φ_F = 4.0 %).[19]

The comparison of the emission properties of compounds **7** and **8** sheds some light into the contribution of an ESIPT mechanism to the deactivation pathways in **7**. The dual emission behavior of **7** is in contrast to the emission of the parent fluorophores, 3-substituted 2-(oxazolinyl)phenols,[42] which only exhibit a single band at *ca.* 480 nm corresponding to the keto form generated through ESIPT. Importantly, the dual emission behavior of **7** indicates that the energy barrier between the enol and the keto form of the terminal fluorophores is large[44] due to solvent-induced interactions.[45,46] Thus, this feature can tentatively be assigned to the coupling of two competing processes at the terminal fluorophores, an excited-state charge transfer and ESIPT. These experimental observations are in agreement with DFT calculations (*vide infra*); the LUMOs involved in the main transitions in the enol form show that the charge partially moves towards the helicene system (*Figures S40* and *S41*), indicating that the extended π-system of the helicene unit acts as an electron-withdrawing group in the excited state. We thus investigated further the photophysical properties of **7** in terms of the competing excited-state processes. To confirm this behavior, we acquired the emission spectrum of **7** in methanol (MeOH; *Figure 1,a*), a solvent with a marked proton-donor character. Solvation of the terminal fluorophores in MeOH involves hydrogen bonding with the hydroxy groups and the nitrogen atoms of the oxazolinyl groups, which deactivates ESIPT.[47] Indeed, the emission spectrum of **7** in MeOH shows mainly the blue, vibronically structured band, and much less dominance of the red shoulder originating from the keto from. As expected, the emission spectrum of **8** in MeOH did not show significant differences (*Figure 1,b*), confirming that hydrogen bonding with the solvent does not influence the emission of the chromophore in which ESIPT is not feasible.

Although the ESIPT processes are usually very fast, even down to fs timescale, the large energy barrier between the enol and the keto form, which results in the dual emission behavior, enables the detection of both forms. The excited-state population deactivation dynamics in the nanosecond time regime thus allows to deconvolute the contribution of the different emissive species to the overall spectrum using time-resolved fluorimetry. Time-resolved emission spectra (TRES) of compounds **7** and **8** were acquired in both MeOH and CH_2Cl_2. Compound **7** displays three decay components along the whole emission range in CH_2Cl_2, with the decay times of 8.83 ± 0.01, 3.37 ± 0.01, and 1.27 ± 0.01 ns. To dissect the contribution of the different emissive components, the extraction of the species-associated emission spectra (SAEMS) was performed (*Figure 1,c*). Two very distinct emissive species

 © 2022 The Authors. Helvetica Chimica Acta Published by Wiley-VHCA AG

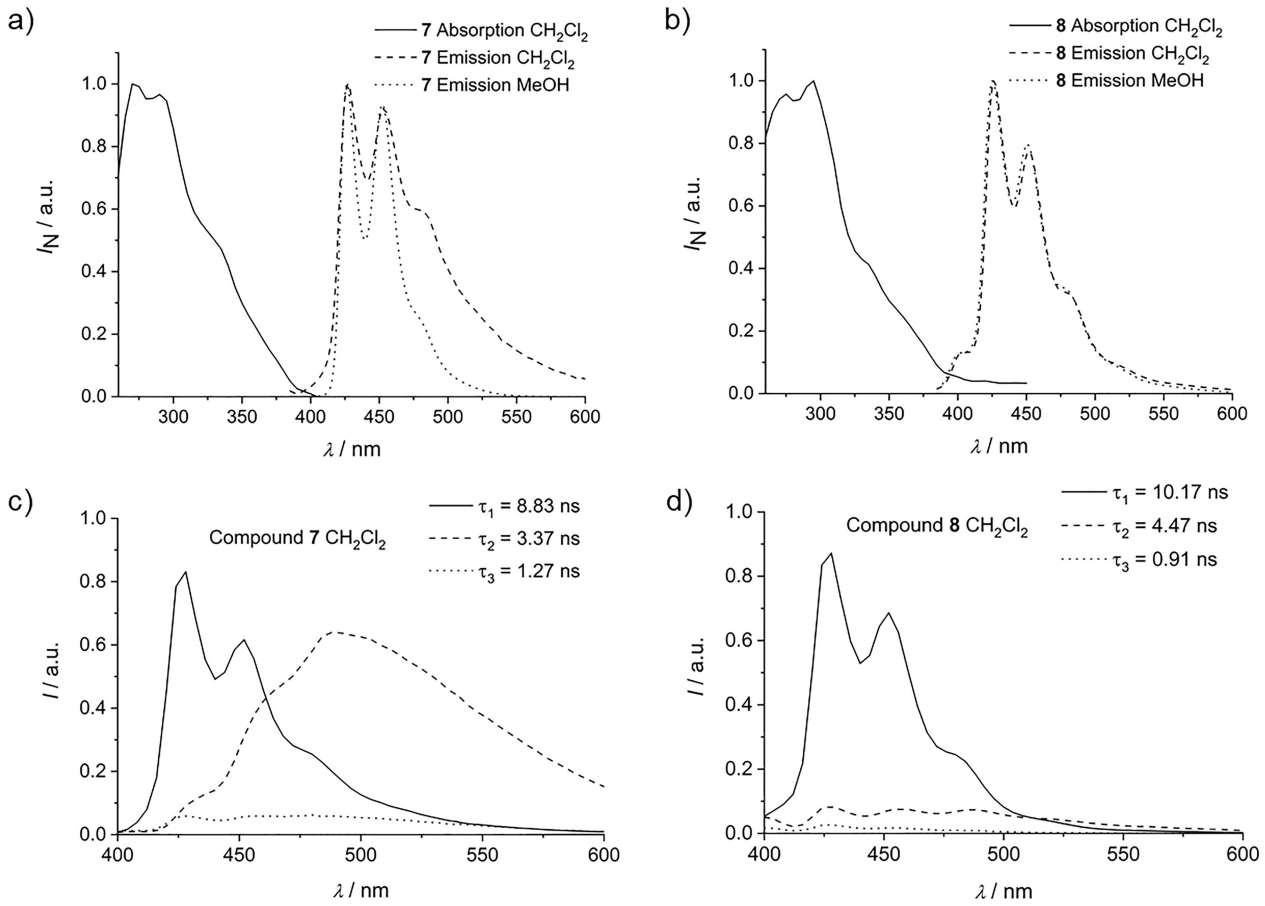

Figure 1. Top: Normalized UV-Vis absorption and steady-state emission spectra of **7** (a) and **8** (b) in CH_2Cl_2 and MeOH. Bottom: Species-associated emission spectra (SAEMS) of compounds **7** (c) and **8** (d) in CH_2Cl_2.

were discriminated in **7**, a long-lifetime form (8.83 ns) exhibiting the blue vibronic band and an intermediate-lifetime form (3.37 ns) emitting in the broad-red-band range peaking at 500 nm. Interestingly, the minor, short component (1.27 ns) shows contributions of both forms, suggesting reversible equilibrium kinetics.

In contrast to CH_2Cl_2, compound **7** in MeOH shows one main component, namely, the blue-shifted, structured band with a decay time of 7.81 ± 0.01 ns (*Figure S1*). The intermediate- (1.98 ± 0.01 ns) and short-decay-time (0.28 ± 0.01 ns) components were minor and show contribution also in the 450–475 nm region, with a negligible contribution > 500 nm. This clearly supports that ESIPT is suppressed in MeOH on account of hydrogen bonding. This behavior is very similar to that of compound **8**, which exhibits one main, long-lived component in both solvents (10.17 ns in CH_2Cl_2, *Figure 1,d* and 9.97 ns in MeOH, *Figure S2*), and two minor, intermediate- and short-lived, components with contributions along the emission band.

Chiral resolution of **7** and **8** was achieved by using chiral-stationary-phase (CSP)-HPLC (for details, see the *Experimental Section* and the *Supporting Information*). Chromatographic separation led to isolation of **7** as two enantiopure (> 99 % e.e.) compounds. In contrast, resolution of the non-hydroxylated helicene **8** was more cumbersome, yielding enantioenriched mixtures with 40 % e.e. (for details, see the *Supporting Information*, *Figures S45–S50*). Both compounds **7** and **8** show configurational stability after resolution and racemize neither thermally (at room temperature) nor upon UV-Vis irradiation.

Electronic circular dichroism (ECD) spectra of the enantiomers of **7** and **8** were measured in CH_2Cl_2 and are depicted in *Figure 2a,b*. The first HPLC fraction (t_R = 13.9 min) of **7** shows a positive *Cotton* effect at 310 nm and a negative *Cotton* effect at wavelengths above 343 nm, including the lowest energy transition

 © 2022 The Authors. Helvetica Chimica Acta Published by Wiley-VHCA AG

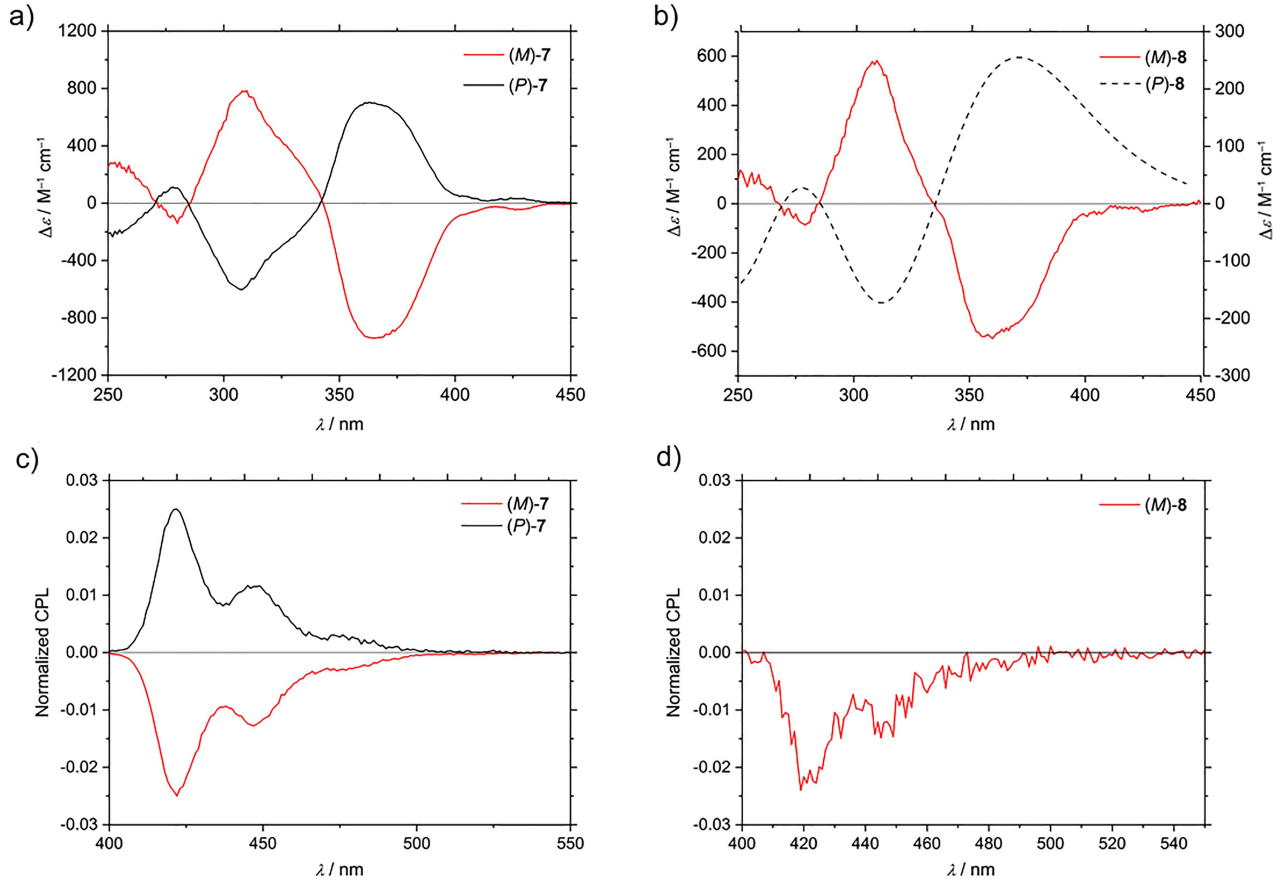

Figure 2. Top: Experimental ECD spectra of enantiomers (*P*)- and (*M*)-**7** (a), and (*M*)-**8** (b) in CH_2Cl_2. The calculated ECD spectrum for (*P*)-**8** (dashed line) has a correction of −0.5 eV for the wavelength to match the experimental spectrum of (*M*)-**8**. Bottom: Normalized CPL spectra of enantiomers (*P*)- and (*M*)-**7** (c), and (*M*)-**8** (d) in CH_2Cl_2. Only (*M*)-**8** is included (d) as second CSP-HPLC fraction showed an impurity.

at 428 nm. The second HPLC fraction ($t_R = 15.2$ min) exhibits a mirror-image spectrum with a negative band centered at 310 nm and a positive *Cotton* effect at wavelengths above 343 nm. Values of $\Delta\varepsilon$ reach maxima between 600 and 1000 $M^{-1}cm^{-1}$, which is in the range of values obtained for many simple and multiple [6]helicenes.[48,49] Similar band pattern and $\Delta\varepsilon$ values were obtained for the first enantioenriched HPLC fraction of **8**. Absorption dissymmetry factors g_{abs} calculated from the experimental spectroscopic data reached outstanding values of 0.011 at 312 nm and 0.019 at 308 nm for (*M*)-**8** and (*M*)-**7**, respectively.

The theoretical UV-Vis and ECD spectra of **7** and **8** were calculated at the B3LYP/6-31G(d,p) level of DFT calculation in vacuum using Gaussian 09.[50] In addition, calculations were performed using the polarizable continuum model (PCM) for solvents of different polarity such as cyclohexane and methanol and hybrid functionals with higher HF contribution such as CAM–B3LYP and M06-2X (*Figures S3–S40*). In every case, the results predict the same absolute configuration and computed ECD band profiles match well the experimental data (*Figures S3* and *S4*), which allows the first HPLC fractions of **7** and **8** to be assigned as the (*M*)-enantiomer whilst the second fractions are (*P*)-configured (for more details, see *Supporting Information*). Furthermore, although the experimental $|g_{abs}|$ values for the lowest-energy transition could not be estimated due to low absorption of both enantiopure samples at the longest absorption wavelength, the calculations predict quite remarkable $|g_{abs}|$ values in the range of 10^{-2} for the $S_0 \rightarrow S_1$ transition for both **7** (0.034) and **8** (0.030).[51] Since fluorescence of helicenes usually occurs from the lowest excited state (S_1), the g_{lum} factor generally correlates with the g_{abs} for the lowest-energy transition. A general trend of $g_{lum} \leq g_{abs}$ is observed for organic molecules with a factor of 0.61 described for helicenes ($|g_{lum}| = 0.61 \times |g_{abs}|$).[12]

 © 2022 The Authors. Helvetica Chimica Acta Published by Wiley-VHCA AG

To our delight, the experimental maximum $|g_{lum}|$ values reached 0.025 at 418 nm and 0.024 at 413 nm for (*M*)-**7** and (*M*)-**8**, respectively, which entails up to a 25-fold amplification of the $|g_{lum}|$ value with respect to the simplest [6]helicene (0.001)[51] by a simple structural modification. It is important to note that the CPL emission profiles are very similar to that of the long-lived species for both compounds (decay time of 8.83 and 10.17 ns for **7** and **8**, respectively, *Figure 1c,d*). This suggests that CPL arises mainly from this form and that the CPL emission is generated in the transition that is associated with the charge-transfer species in which electron charge is partially localized on the helicene moiety.

Next, we examined whether exciton coupling between the chromophores in closest proximity, namely, two oxazoline units pending at the periphery of the central helicene core, is the reason for such large dissymmetry factors. The DFT calculations for (*M*)-**7** and (*M*)-**8** performed at the CAM–B3LYP/6-31G(d,p) level of theory were therefore analyzed in terms of molecular orbitals (MOs), with a predominant contribution to the first five low-energy transitions (*Figures S41–S44*), and their energies, along with the comparison of oscillator (*f*) and rotational strengths (*R*) (*Tables S1* and *S2*). Compound (*M*)-**7** exhibits two excitations (#3 and #5) with intense rotatory strengths of almost the same dimension but opposite sign, separated by *ca.* 30 nm (*Table S1*), which could be indicative of the exciton coupling between the terminal oxazolines. When looking at the MOs with dominant contribution to those two excitations, however, there is only a partial shift of the charge from the periphery to the helicene core (*Figure S41*, HOMO−1 to LUMO+1, *Figure S42*, HOMO to LUMO+1). This small shift, together with the high energies of these transitions (3.84 and 4.26 eV), suggests that in case an exciton coupling is taking part, it is to a lesser extent than previously described for 2,15-disubstituted [6]helicenes.[21] Compound (*M*)-**8** exhibits analogous excitations (*Table S2*, 3.96 and 4.40 eV), with the only difference being a partial charge shift, in this case from the helicene core to the peripheral oxazoline units (*Figure S43*, HOMO−1 to LUMO+1, *Figure S44*, HOMO to LUMO+1). Thus, also for (*M*)-**8**, the contribution of the exciton coupling to the chiroptical response is expected to be minor.

In homogeneous solutions, the dissymmetry factor g_{abs} can be expressed theoretically in terms of the electric (μ) and magnetic (*m*) transition dipole moments using the simplified equation $g_{abs} \approx 4 \cdot |m| \cdot \cos\theta / |\mu|$ for a particular transition.[48] Therefore, the g_{abs} values that are considerably high for simple [6]helicenes like **7** and **8** can be ascribed to the abnormally small calculated electric transition dipole moment (μ), relatively large calculated magnetic transition dipole moment (*m*), and angles between both transition dipole moments (θ) of either $<30°$ or $>170°$ in both cases. Thereby, for the $S_0 \rightarrow S_1$ transition, values of $|\mu| = 93 \cdot 10^{-20}$ esu cm, $|m| = 0.85 \cdot 10^{-20}$ erg G^{-1}, and $|\theta| = 22°$ were obtained for **7** and values of $|\mu| = 150 \cdot 10^{-20}$ esu cm, $|m| = 1.1 \cdot 10^{-20}$ erg G^{-1}, and $|\theta| = 20°$ were obtained for **8**, leading to partially electrically forbidden transitions and optimum close-to-parallel-oriented μ and *m* vectors.

The photophysical results show that incorporation of the ESIPT units into a CPL-active [6]helicene is a suitable strategy to combine both phenomena. As expected, the incorporation of the oxazoline moieties leads to large *Stokes* shifts for both the doubly hydroxylated [6]helicene **7** (~13,600 cm^{-1}) and the non-hydroxylated control compound **8** (~10,400 cm^{-1}). Besides, in **7**, a red shift of the emission is observed, concurrent with the dual emission behavior on account of the coexistence of a keto emissive form (shoulder at *ca.* 500 nm in the emission spectrum) arising from an ESIPT reaction and an enol species in which the charge is transferred towards the helicene unit, making the emission active in CPL. Contrary to our initial expectations, the values of the quantum yields were found to be rather low, indicating that boosting of emission efficiency is extremely challenging and requires further improvement of the molecular design. The most remarkable observation during this study is the exceptionally high chiral response of [6]helicenes **7** and **8** with g_{lum} values of the same order of magnitude as the most potent literature examples (*Scheme 1,a–c*). In addition, a factor to be taken into account when assessing emission performance is the recently introduced concept of CPL-brightness or luminosity (B_{CPL}),[52,53] which depends on molar absorption extinction coefficient ($\varepsilon_{\lambda exc}$), quantum yield ($\Phi_F$) and g_{lum} through the equation $B_{CPL} = \varepsilon_{\lambda exc} \times \Phi_F \times |g_{lum}|/2$. In this regard, compounds **7** and **8** display B_{CPL} values of 56 and 73 $M^{-1} cm^{-1}$, respectively, which are significantly higher than that of the simplest carbo[6]helicene (~2 $M^{-1} cm^{-1}$)[54] as well as the average value (18.7 $M^{-1} cm^{-1}$) described for helicenes and helicenoids.[52]

 © 2022 The Authors. Helvetica Chimica Acta Published by Wiley-VHCA AG

Conclusions

Two [6]helicenes decorated with oxazoline moieties at both ends were synthesized in good yields through a five-step pathway including photocyclization and cross-coupling reactions as the key steps. The inclusion of two hydroxy groups *ortho* to the oxazoline units in compound **7** was found to be key for the excited-state intramolecular proton transfer (ESIPT) process leading to a characteristic red-shifted emission. Both racemic compounds **7** and **8** were resolved by means of chiral-stationary-phase HPLC, and photophysical investigations of enantiopure compounds in case of **7** and enantioenriched samples for **8** revealed very similar dissymmetry factors for absorbance and emission (g_{abs} and g_{lum}) for both compounds. Remarkably, exceptionally high g_{abs} of up to 10^{-2} were obtained from the experimental CD and absorbance, and these values were in a good agreement with those calculated at the B3LYP/6-31G (d,p) level of theory for the longest-wavelength transitions. An explanation for this observation is the low μ modules and the angles (θ) between μ and m maximizing the cosine of θ. In addition, outstanding g_{lum} values of *ca.* 10^{-2} were achieved, corresponding to a 25-fold amplification with respect to the simplest [6]helicene. The red-shifted emission of the doubly hydroxylated [6]helicene **7** along with its outstanding g_{abs} and g_{lum} ($\approx 10^{-2}$), large *Stokes* shift of 13,600 cm^{-1}, and CPL-brightness (B_{CPL}) nominates this simple chiral molecule as a promising candidate for its implementation in materials and posterior use in optoelectronics applications.

Experimental Section

General Information

Unless stated otherwise, all reactions were carried out under a nitrogen atmosphere using standard *Schlenk* techniques. All chemicals and solvents were purchased from commercial suppliers and either used as received or purified according to 'Purification of Common Laboratory Chemicals'.[55] Yields refer to yields of isolated compounds estimated to be >95% pure as determined by ^{1}H-NMR spectroscopy.

NMR Spectra were recorded on a *Bruker AV2-400* with a *QNP* (5 mm) probe head at 23 °C. Chemical shifts for ^{1}H-NMR spectra are reported as δ (parts per million, ppm) relative to the residual proton signal of $CDCl_3$ at 7.26 ppm (*s*). Chemical shifts for $^{13}C\{^1H\}$-NMR spectra are reported as δ (parts per million, ppm) relative to the signal of $CDCl_3$ at 77.0 ppm (*t*). ^{31}P-NMR spectra are reported as δ (parts per million, ppm) relative to the signal of $Si(CH_3)_4$ at 0.0 ppm. The following abbreviations are used to describe splitting patterns: br. = broad, *s* = *singlet*, *d* = *doublet*, *dd* = *doublet* of *doublets*, *m* = *multiplet*. Coupling constants *J* are given in Hertz [Hz].

Thin-layer chromatography was performed on fluorescence-indicator-marked precoated silica gel *60* plates (*Macherey-Nagel*, *ALUGRAM Xtra SIL G/UV254*) and visualized by UV light (254 nm/366 nm). Flash column chromatography was performed on silica gel (0.040–0.063 mm) with the solvents given in the procedures. Abbreviations for solvents used: CH = cyclohexane, CH_2Cl_2 = dichloromethane. Retention factors were determined at chamber saturation at 23 °C. Developments were carried out between 3.0–3.5 cm.

High-resolution (HR)-EI mass spectra were recorded on a double focusing (BE geometry) magnetic sector mass spectrometer *DFS* from *ThermoFisher Scientific*. HR-ESI mass spectra were recorded on a *timsTOF Pro* TIMS-QTOF-MS instrument from *Bruker Daltonics*. All signals are reported with the quotient from mass to charge *m/z*.

IR Spectra were recorded on a *Perkin Elmer Spectrum Two* spectrometer with a diamond ATR unit. The absorption bands are reported in cm^{-1} with indicated relative intensities: *s* (strong, 0–33% *T*); *m* (medium, 34–66% *T*), *w* (weak, 67–100% *T*). *T* = transmission.

Melting points of solids, compounds that solidified after chromatography, were measured on a *Büchi M-560* Melting Point apparatus and are uncorrected. The measurements were performed with a heating rate of 5 °C/min and the melting points are reported in °C.

Absorption measurements were performed using an *Agilent 8453* UV-Vis spectrophotometer. Emission measurements were performed using an *Edinburgh Instruments FS5* spectrofluorometer with a *SC-25* temperature controlled holder and a *TE*-cooled-standard cell. Absolute quantum yields were measured using an *Edinburgh SC-30* integrating sphere. All measurements were performed at 23 °C in quartz cuvettes with 10 mm path length by *Hellma Analytics*.

 © 2022 The Authors. Helvetica Chimica Acta Published by Wiley-VHCA AG

Enantiopure materials were obtained by chiral-stationary-phase HPLC resolution on an *Agilent 1260 Infinity II* apparatus (quaternary pump, auto sampler, column thermostat, and a diode-array detector) using a semi-preparative *CHIRALPAK® IA* column (250× 10 mm, 5 μm) at a flow rate of 1 mL/min (injection volume = 250 μL) for **7** and with an analytical *CHIRALPAK® IC* column (250×4.6 mm, 5 μm) at a flow rate of 1 mL/min (injection volume 25 = μL) for **8** and HPLC grade solvents.

Both the electronic circular dichroism (ECD) and circularly polarized luminescence (CPL) spectra were recorded with an *Olis DSM172* spectrophotometer. ECD Spectra are an average calculated for 56 and 3 scans for **8** and **7**, respectively, and for CPL spectra, an average of 13 scans for **8** and 20 scans for **7** were recorded. For ECD and CPL measurements, fixed 0.1 s and 1.0 s of integration time, respectively, were selected. The spectra were recorded at approximately 10^{-5} M concentrations in HPLC-grade solvents at room temperature. A fixed wavelength of 370 nm provided by a LED source was employed when measuring CPL.

Steady-state emission spectra were collected using a *JASCO FP-8500* spectrofluorometer with 5×10 mm cuvettes.

Time-resolved fluorescence decay traces were collected through the time-correlated single photon counting (TCSPC) method using a *FluoTime 200* fluorometer (*PicoQuant, GmbH*). The excitation source was a 375-nm pulsed diode laser (*LDH-P-C-375B PicoQuant, GmbH*), being around 40 ps the full width at half maximum (fwhm) of the laser pulses and using a 10 MHz excitation frequency.

The fluorescence emission was collected at a 90° geometry, focused at the detector after crossing through a polarizer (set at the magic angle), 2-mm slits, and a 2-nm bandwidth monochromator. TCSPC was achieved by a *TimeHarp200* board, set at 36 ps/channel. The histogram of the instrument response function (IRF) was determined using a LUDOX scatterer. Fluorescence decay traces were collected for the necessary time to reach 20,000 counts at the peak channel.

Time-resolved emission spectroscopy (TRES) of compounds **7** and **8** in CH_2Cl_2 and methanol was performed by collecting 52 fluorescence decay traces in the 400–600 nm emission range ($\Delta\lambda_{em} = 4$ nm). In order to maintain the overall intensity information, the decay traces were collected during a fixed amount of time (200 s).

The fluorescence decay traces were fitted to a three-exponential function by using a *Levenberg–Marquardt* algorithm-based nonlinear least-squares error minimization iterative reconvolution method (FluoFit 4.4 package, *Picoquant GmbH*). For the time-resolved emission spectroscopy (TRES) analysis and the estimation of the species-associated emission spectra (SAEMS), the 52 decay traces were fitted globally with the decay times linked as shared parameters, whereas the pre-exponential factors were local adjustable parameters. The quality of fittings was assessed by the value of the reduced chi-squared, χ^2, parameter and random distributions of the weighted residuals and the autocorrelation functions.

The SAEMS of each species *i* at any given emission wavelength ($SAEMS_i(\lambda_{em})$) is given by the fluorescence intensity emitted by the species *i* ($A_{i,\lambda_{em}} \times \tau_i$), normalized by the total intensity and corrected for the different detection sensitivity using the total intensity of the steady-state spectrum ($I_{ss,\lambda_{em}}$) as shown in *Eqn. 1*:

$$SAEMS_i(\lambda_{em}) = \frac{A_{i,\lambda_{em}} \times \tau_i}{\sum_i A_{i,\lambda_{em}} \times \tau_i} \cdot I_{ss,\lambda_{em}} \quad (1)$$

Figures 1c,d, *S1* and *S2* show the SAEMS of compounds **7** and **8** dissolved in CH_2Cl_2 and methanol.

Syntheses

Naphthalene-2,7-dicarbaldehyde (**9**). A slightly modified literature procedure was used.[56] A heat gun-dried and nitrogen-flushed *Schlenk* flask (1 L) equipped with a dropping funnel on top was charged with 2,7-dibromonaphthalene (12.6 g, 44.0 mmol, 1.0 equiv.) and anhydrous THF (400 mL, 0.1 M), and the solution was transferred through cannula through the dropping funnel into the reaction flask. The solution was cooled to −78 °C (dry ice/acetone bath) and *tert*-butyllithium (102 mL, 194 mmol, 4.4 equiv., 1.9 M in pentane) was transferred through a cannula into the dropping funnel and added dropwise over 40 min (~2.6 mL/min) to the vigorously stirred mixture. After complete addition, the mixture was stirred for 30 min under the same conditions to give a deep red solution (during addition, the solution turned from pale red to dark red). Next, the dropping funnel was rinsed with anhydrous THF (15 mL) to remove remaining *tert*-

 © 2022 The Authors. Helvetica Chimica Acta Published by Wiley-VHCA AG

butyllithium. Then, anhydrous DMF (27.3 mL, 352 mmol, 8.0 equiv.) was added dropwise through the dropping funnel over 15 min (~1.8 mL/min) at −78 °C, and the mixture was stirred for another 30 min under the same conditions. The turbid mixture was stirred for 18 h while it was allowed to warm slowly to ambient temperature (23 °C). During warming, the brown suspension turned beige/colorless and became very viscous. Saturated NH_4Cl solution (150 mL) and water (50 mL) were added (mixture turned yellow), the phases were separated, and the aqueous phase was extracted with AcOEt (3×100 mL). The combined organic phases were dried over anhydrous $MgSO_4$, filtered, and concentrated under reduced pressure on a rotary evaporator. The yellow crude product was washed with methanol (50 mL) to remove yellow impurities to obtain 2,7-naphthalenedicarbaldehyde **9** in pure form (4.41 g, 23.9 mmol, 54%). The filtrate was concentrated and washed with ice-cooled methanol (30 mL) to achieve another portion of clean product (2.22 g, 12.1 mmol, 27%). In total, naphthalene-2,7-dicarbaldehyde (**9**; 6.63 g, 36.0 mmol, 82%) was obtained as an off-white solid. R_f (CH/AcOEt 5:1 (*v/v*)) 0.11. M.p. 143–145 °C. ^{1}H-NMR (400 MHz, $CDCl_3$): 10.22 (*d*, $^4J_{HH}$ = 0.6, 2 H); 8.54–8.48 (*m*, 2 H); 8.12 (*dd*, $^3J_{HH}$ = 8.6, $^4J_{HH}$ = 1.5, 2 H); 8.06–7.99 (*m*, 2 H). ^{13}C{^{1}H}-NMR (101 MHz, $CDCl_3$): 191.7; 139.5; 135.4; 135.2; 132.3; 129.5; 126.2. IR (ATR, neat): 2852*w*, 1683*s*, 1629*m*, 1576*w*, 1509*w*, 1465*w*, 1439*w*, 1409*w*, 1396*w*, 1374*w*, 1329*m*, 1269*m*, 1254*w*, 1209*m*, 1183*w*, 1154*m*, 1119*w*, 1009*w*, 978*w*, 914*w*, 850*s*, 816*m*, 782*m*, 745*m*, 721*w*, 640*w*, 614*w*, 585*w*, 529*w*, 508*w*. HR-EI-MS: 183.04404 ($C_{12}H_7O_2^+$, $[M-H]^+$; calc. 183.04406, Dev.: −0.02 mu; −0.11 ppm). The analytical data are in accordance with the literature.[57]

[(4-Bromophenyl)methyl](triphenyl)phosphanium Bromide (**10**). A literature procedure was used.[58] 4-Bromobenzyl bromide (10.2 g, 40.0 mmol, 1.0 equiv.) and triphenylphosphine (11.5 g, 44.0 mmol, 1.1 equiv.) were dissolved in toluene (160 mL, 0.25 M) and heated at 120 °C. During warming, product precipitation was observed. After stirring for 18 h under these conditions, the mixture was cooled to ambient temperature (23 °C). The precipitate was filtered off, washed with toluene (100 mL), and dried *in vacuo* at 50 °C to afford **10** (20.5 g, 39.9 mmol, 99%) as a colorless solid. M.p. 280–282 °C. ^{1}H-NMR (400 MHz, $CDCl_3$): 7.81–7.67 (*m*, 9 H); 7.62–7.53 (*m*, 6 H); 7.19–7.11 (*m*, 2 H); 7.10–7.01 (*m*, 2 H); 5.57 (*d*, $^2J_{HP}$ = 14.8, 2 H). ^{13}C{^{1}H}-NMR (101 MHz, $CDCl_3$): 135.0 (*d*, *J* = 3.0); 134.6 (*d*, *J* = 10.1); 133.5 (*d*, *J* = 5.4); 131.8 (*d*, *J* = 3.0); 130.2 (*d*, *J* = 12.5); 126.7 (*d*, *J* = 8.9); 122.7 (*d*, *J* = 5.4); 117.7 (*d*, *J* = 85.8); 29.9 (*d*, *J* = 46.5). ^{31}P-NMR (162 MHz, $CDCl_3$): 23.2 (*s*). IR (ATR, neat): 3033*w*, 3009*w*, 2974*w*, 2858*w*, 2785*w*, 1584*w*, 1488*m*, 1437*m*, 1413*m*, 1402*w*, 1330*w*, 1315*w*, 1243*w*, 1189*w*, 1166*w*, 1108*s*, 1074*m*, 1028*w*, 1013*m*, 994*m*, 941*w*, 862*m*, 833*m*, 820*m*, 771*m*, 753*m*, 744*m*, 718*s*, 710*m*, 701*m*, 685*s*, 625*m*, 528*s*, 510*s*. HR-ESI-MS: 431.05609 ($C_{25}H_{21}BrP^+$, M^+; calc. 431.05588, Dev.: 0.21 mu; 0.48 ppm). The analytical data are in accordance with the literature.[59]

2,7-Bis[2-(4-bromophenyl)ethenyl]naphthalene (**11**). A modified literature procedure was used.[60] A heat-gun-dried and nitrogen-flushed *Schlenk* flask was charged with **10** (28.0 g, 54.6 mmol, 2.1 equiv.) and anhydrous THF (120 mL; 0.46 M) was added to give a suspension. Potassium *tert*-butoxide (53.3 mL, 53.3 mmol, 2.05 equiv.; 1.0 M in THF) was added through a syringe pump (2.5 mL/min) through a rubber septum at 23 °C. After complete addition, the deep-orange mixture was stirred at 23 °C for 1 h. Then, **9** (4.79 g, 26.0 mmol, 1.0 equiv.) dissolved in anhydrous THF (80 mL; 0.33 M) was added dropwise through a syringe pump (3.5 mL/min). The deep orange color disappeared partially to give a pale-orange suspension. The suspension was stirred at ambient temperature (23 °C) for 18 h. The dialdehyde was consumed after this time and the mixture was concentrated under reduced pressure on a rotary evaporator. The crude, partially orange solid was triturated in an ice-cooled methanol/water mixture (100 mL, 5:2 (*v/v*)), filtered, and washed successively with water (100 mL) and ice-cooled methanol (50 mL) to yield the product contaminated with triphenylphosphine oxide (TPPO) as a pale-yellow solid. To get rid of TPPO, the crude product was suspended in CH_2Cl_2 and filtered over a plug of silica gel. Flushing with CH_2Cl_2 provided **11** (10.7 g, 21.9 mmol, 84%) as a mixture of isomers and as an off-white solid. If desired, the (*E,E*)-stereoisomer can be isolated by flash column chromatography (CH/AcOEt 100:1 (*v/v*)) as a colorless solid. R_f (CH_2Cl_2) 0.93. R_f (CH/AcOEt 100:1 (*v/v*)) 0.28. M.p. 182–196 °C (very slow melting). ^{1}H-NMR (400 MHz, $CDCl_3$): 7.63–7.57 (*m*, 4 H); 7.38–7.30 (*m*, 4 H); 7.28 (*dd*, $^3J_{HH}$ = 8.4, $^4J_{HH}$ = 1.7, 2 H); 7.17–7.12 (*m*, 4 H); 6.76 (*d*, $^3J_{HH}$ = 12.2, 2 H); 6.58 (*d*, $^3J_{HH}$ = 12.1, 2 H). ^{13}C{^{1}H}-NMR (101 MHz, $CDCl_3$): 136.2; 134.9; 133.6; 131.9; 131.5; 130.9; 130.7; 129.5; 128.2; 127.6; 127.1; 121.3. IR (ATR, neat): 3011*m*, 2967*m*, 2923*m*, 1905*m*, 1710*m*, 1622*m*, 1599*m*, 1583*m*, 1515*m*, 1483*s*, 1427*m*, 1402*m*, 1346*m*, 1231*m*, 1174*m*, 1153*m*, 1124*m*, 1101*m*, 1070*s*, 1010*s*,

 © 2022 The Authors. Helvetica Chimica Acta Published by Wiley-VHCA AG

969*s*, 958*m*, 949*m*, 910*s*, 883*m*, 869*s*, 845*s*, 824*s*, 812*s*, 801*s*, 784*m*, 771*m*, 746*s*, 708*m*, 643*m*, 630*m*, 597*m*, 571*m*, 560*m*, 529*m*, 513*s*. HR-EI-MS: 487.97699 ($C_{26}H_{18}Br_2^+$, M^+; calc. 487.97698, Dev.: 0.01 mu; 0.03 ppm). The analytical data are in accordance with the literature.[61]

2,15-Dibromohexahelicene (**12**): A slightly modified literature procedure was used.[43] The reaction was carried out in a 700 mL photo-reactor system (150 W mercury lamp). Compound **11** (172 mg, 350 μmol, 1.0 equiv.) was dissolved in toluene (700 mL; 0.5 mM) and elemental iodine (199 mg, 770 μmol, 2.2 equiv.) and methyl oxirane (12.3 mL, 175 mmol, 500 equiv.) were added successively. The red solution was bubbled with an argon-filled balloon for 30 min while stirring. The balloon was removed, and the photo-reactor was started. After 90 min, the reaction was stopped, and no more starting material was observed by TLC. The slightly turbid, red mixture was transferred into a large round-bottom flask using AcOEt to clean the photo-reactor vessel, saturated $Na_2S_2O_3$ solution (1 mL) was added, and the suspension was concentrated under reduced pressure on a rotary evaporator. Within 10 min, the remaining iodine was reduced to give a yellow/colorless suspension. This procedure was performed six times and the combined crude products were subjected to purification. The residue was washed with ice-cooled methanol/water (100 mL, 1:1 (*v/v*)) and with cyclohexane (30 mL) to yield **12** as a pale yellow solid (991 mg, 2.0 mmol, 97%). Average yield: 165 mg, 339 μmol, 97%. R_f (CH/AcOEt 10:1 (*v/v*)) 0.50. M.p. 293 °C (decomp.). ^{1}H-NMR (400 MHz, $CDCl_3$): 8.04 (*d*, $^3J_{HH}$ = 8.2, 1 H); 8.00 (*d*, $^3J_{HH}$ = 8.2, 1 H); 7.96 (*d*, $^3J_{HH}$ = 8.6, 1 H); 7.91 (*d*, $^3J_{HH}$ = 8.6, 1 H); 7.74 (*d*, $^3J_{HH}$ = 8.5, 1 H); 7.71 (*d*, $^4J_{HH}$ = 1.8, 1 H); 7.39 (*dd*, $^3J_{HH}$ = 8.5, $^3J_{HH}$ = 1.9, 1 H). ^{13}C{^{1}H}-NMR (101 MHz, $CDCl_3$): 133.3; 132.0; 130.9; 130.8; 130.1; 129.4; 129.1; 127.8; 127.7; 127.5; 126.9; 126.5; 123.9; 119.4. IR (ATR, neat): 3049*m*, 3013*m*, 2923*m*, 2853*m*, 1617*m*, 1582*m*, 1511*m*, 1486*m*, 1400*m*, 1349*m*, 1305*m*, 1289*m*, 1251*m*, 1119*m*, 1104*m*, 1075*s*, 1008*s*, 968*s*, 953*m*, 918*m*, 892*m*, 855*m*, 844*s*, 835*s*, 814*s*, 768*m*, 749*m*, 733*m*, 708*m*, 664*m*, 636*m*, 623*m*, 587*s*, 558*m*, 530*m*, 509*m*. HR-EI-MS: 483.94602 ($C_{26}H_{14}Br_2^+$, M^+; calc. 483.94568, Dev.: 0.34 mu; 0.71 ppm). The analytical data are in accordance with the literature.[61]

4,4-Dimethyl-2-[4-(4,4,5,5-tetramethyl-1,3,2-dioxaborolan-2-yl)phenyl]-4,5-dihydro-1,3-oxazole (**13**). A slightly modified literature procedure was used.[62] A heat-gun-dried and nitrogen-flushed *Schlenk*-tube was charged with 2-(4-bromophenyl)-4,4-dimethyl-4,5-dihydro-1,3-oxazole[63] (2.54 g, 10.0 mmol, 1.0 equiv.), B_2pin_2 (2.79 g, 11.0 mmol, 1.1 equiv.), KOAc (2.94 g, 30.0 mmol, 3.0 equiv.), Pd(dppf)Cl_2 (153 mg, 500 μmol, 0.05 equiv.), and anhydrous 1,4-dioxane (40 mL, 0.25 M). The mixture was bubbled with argon for 20 min and then heated at 80 °C and stirred for 18 h under the same conditions. After cooling to ambient temperature, the mixture was diluted with CH_2Cl_2 (40 mL), and saturated NH_4Cl solution (40 mL) and water (20 mL) were added. The phases were separated, and the aqueous phase was extracted with CH_2Cl_2 (3×20 mL). The combined organic phases were dried over anhydrous $MgSO_4$, filtered, and concentrated under reduced pressure on a rotary evaporator. The brown crude product was adsorbed on silica gel and purified by flash column chromatography (CH/AcOEt 5:1 (*v/v*)) to obtain **13** (2.95 g, 9.79 mmol, 98%) as a crystalline, colorless solid. R_f (CH/AcOEt 5:1 (*v/v*)) 0.20. M.p. 132–134 °C. ^{1}H-NMR (400 MHz, $CDCl_3$): 7.96–7.89 (*m*, 2 H); 7.86–7.80 (*m*, 2 H); 4.11 (*s*, 2 H); 1.39 (*s*, 6 H); 1.35 (*s*, 12 H). ^{13}C{^{1}H}-NMR (101 MHz, $CDCl_3$): 134.8 (2×); 127.5; 84.2; 79.3; 67.7; 28.5; 25.0 (two carbon resonances were not detected because of signal broadening due to boron quadrupole coupling). IR (ATR, neat): 2976*m*, 2929*w*, 2891*w*,1648*m*, 1613*w*, 1558*w*, 1516*w*, 1462*w*, 1400*m*, 1360*s*, 1348*s*, 1327*m*, 1313*m*, 1301*m*, 1286*m*, 1270*m*, 1211*m*, 1187*m*, 1174*m*, 1141*s*, 1091*s*, 1058*s*, 1018*s*, 988*w*, 962*m*, 920*w*, 853*s*, 819*m*, 743*w*, 693*s*, 667*m*, 653*s*, 617*w*, 578*w*, 547*w*, 521*w*. HR-ESI-MS: 302.19169 ($C_{17}H_{25}BNO_3^+$, $[M+H]^+$; calc. 302.19220, Dev.: −0.51 mu; −1.68 ppm).

2,2′-[Hexahelicene-2,15-diyldi(4,1-phenylene)]bis(4,4-dimethyl-4,5-dihydro-1,3-oxazole) (**8**). A slightly modified literature procedure was used.[64] A heat-gun-dried and nitrogen-flushed *Schlenk*-tube was charged with compound **12** (243 mg, 500 μmol, 1.0 equiv.), compound **13** (376 mg, 1.25 mmol, 2.5 equiv.), and 1,4-dioxane (10 mL; 0.05 M). K_2CO_3 (518 mg, 3.75 mmol, 7.5 equiv.) was dissolved in distilled water (2 mL) and added to the reaction vessel. Finally, $Pd(PPh_3)_4$ (58.2 mg, 50.0 μmol, 0.1 equiv.) and SPhos (20.5 mg, 50.0 μmol, 0.1 equiv.) were added, and the mixture was bubbled with argon for 20 min. Heating at 100 °C (oil bath temperature) for 24 h resulted in a complete conversion of dibrominated [6]helicene **12**. The reaction mixture was cooled to ambient temperature, diluted with CH_2Cl_2 (20 mL), and saturated NH_4Cl solution (20 mL) and water (20 mL) were added. The phases were separated, and the

 © 2022 The Authors. Helvetica Chimica Acta Published by Wiley-VHCA AG

aqueous phase was extracted with CH_2Cl_2 (3×20 mL). The combined organic phases were dried over anhydrous $MgSO_4$, filtered, and concentrated under reduced pressure on a rotary evaporator. The brown crude product was adsorbed on silica gel and purified by flash column chromatography (CH_2Cl_2/MeOH 100:1 to 50:1 (*v/v*)) to obtain **8** (172 mg, 255 μmol; 51%) as a dark yellow solid. R_f (CH_2Cl_2/MeOH 100:1 (*v/v*)) 0.03. R_f (CH_2Cl_2/MeOH 50:1 (*v/v*)) 0.20. M.p. 333 °C (decomp.). ^{1}H-NMR (400 MHz, $CDCl_3$): 8.12 (*d*, $^4J_{HH}$ = 1.7, 2 H); 8.06–7.96 (*m*, 8 H); 7.94 (*d*, $^3J_{HH}$ = 8.3, 2 H); 7.76 (*d*, $^3J_{HH}$ = 8.2, 4 H); 7.48 (*dd*, $^3J_{HH}$ = 8.3, $^4J_{HH}$ = 1.8, 2 H); 6.84–6.76 (*m*, 4 H); 4.10 (*s*, 4 H); 1.40 (*s*, 6 H); 1.39 (*s*, 6 H). ^{13}C{^{1}H}-NMR (101 MHz, $CDCl_3$): 162.4; 144.0; 137.1; 133.5; 132.1; 131.9; 130.0; 128.5; 128.4 (2×); 128.3; 127.7; 127.5; 127.5; 127.3; 127.2 (2 ×); 127.0; 125.4; 124.1; 79.4; 67.5; 28.5 (two carbon resonances were not detected because of signal overlap). IR (ATR, neat): 3043*w*, 2963*m*, 2925*w*, 2890*w*, 1734*w*, 1645*s*, 1608*m*, 1565*w*, 1499*w*, 1462*w*, 1415*w*, 1383*w*, 1350*m*, 1316*m*, 1302*m*, 1252*w*, 1215*w*, 1184*m*, 1123*w*, 1065*s*, 1017*m*, 991*w*, 966*m*, 918*w*, 872*w*, 845*s*, 833*s*, 785*w*, 748*m*, 738*m*, 688*m*, 672*w*, 653*w*, 630*w*, 621*w*, 610*w*, 567*m*, 538*w*, 510*m*. HR-ESI-MS: 675.30167 ($C_{48}H_{39}O_2N_2^+$, $[M+H]^+$; calc. 675.30060, Dev.: 1.07 mu; 1.57 ppm).

3,3′-(Hexahelicene-2,15-diyl)bis[6-(4,4-dimethyl-4,5-dihydro-1,3-oxazol-2-yl)phenol] (**7**). A literature procedure was used.[63] A heat-gun-dried and nitrogen-flushed *Schlenk*-tube was charged with **8** (67.5 mg, 100.0 μmol, 1.0 equiv.) and anhydrous THF (2.0 mL; 0.05 M). TMPMgCl·LiCl (1.54 mL, 2.00 mmol, 20 equiv.) was added dropwise through syringe through the rubber septum within 1 min. The mixture was stirred for 4 h under these conditions, while the mixture turned orange/brown, but remained clear. Then, an oxygen-filled balloon was placed on top, the reaction vessel was flushed with oxygen, and stirring was continued for another 24 h under ambient conditions. The dark red and clear mixture was diluted with CH_2Cl_2 (20 mL), and saturated NH_4Cl solution (20 mL) and water (10 mL) were added. The phases were separated, and the aqueous phase was extracted with CH_2Cl_2 (3×20 mL). The combined organic phases were dried over anhydrous $MgSO_4$, filtered, and concentrated under reduced pressure on a rotary evaporator. The brown crude product was adsorbed on silica gel and purified by flash column chromatography (CH/AcOEt (4:1 *v/v*) + 0.1% AcOH) to obtain **7** (35.7 mg, 50.5 μmol; 51%) as a dark yellow solid and **8** (10.2 mg, 15.1 μmol; 15%) as a yellow solid. R_f (CH/AcOEt (4:1 *v/v*) + 0.1% AcOH) 0.29. M.p. 187–189 °C. ^{1}H-NMR (400 MHz, $CDCl_3$): 11.85 (br. *s*, 2 H); 8.10 (*d*, $^4J_{HH}$ = 2.0, 2 H); 8.05 (*d*, $^3J_{HH}$ = 8.5, 2 H); 8.02–7.97 (*m*, 6 H); 7.95 (*d*, $^3J_{HH}$ = 8.5, 2 H); 7.50 (*dd*, $^3J_{HH}$ = 8.3, $^4J_{HH}$ = 1.8, 2 H); 7.42 (*d*, $^3J_{HH}$ = 8.1, 2 H); 6.55 (*s*, 2 H); 6.28 (*dd*, $^3J_{HH}$ = 8.1, $^4J_{HH}$ = 1.8, 2 H); 4.11 (*s*, 4 H); 1.40 (*s*, 12 H). ^{13}C{^{1}H}-NMR (101 MHz, $CDCl_3$): 163.9; 160.0; 146.4; 136.9; 133.4; 132.2; 132.0; 129.8; 128.6; 128.3; 127.8; 127.6 (2×); 127.4; 127.3; 126.9; 125.4; 124.1; 117.8; 115.3; 109.0; 78.7; 66.8; 28.5. IR (ATR, neat): 3045*w*, 2965*m*, 2924*m*, 2853*m*, 1899*w*, 1785*w*, 1636*s*, 1620*s*, 1565*m*, 1499*m*, 1477*m*, 1463*m*, 1389*m*, 1376*m*, 1353*m*, 1326*m*, 1309*m*, 1294*m*, 1266*m*, 1192*s*, 1143*m*, 1122*m*, 1068*s*, 1045*m*, 962*m*, 906*m*, 879*m*, 847*s*, 823*s*, 813*s*, 777*s*, 738*m*, 694*m*, 673*w*, 650*w*, 622*m*, 584*w*, 558*m*, 533*w*, 509*m*. HR-ESI-MS: 707.28929 ($C_{48}H_{39}O_4N_2^+$, $[M+H]^+$; calc. 707.29043, Dev.: −1.14 mu; −1.62 ppm).

Acknowledgements

This project received funding from the European Research Council (ERC) under the European Union's Horizon 2020 research and innovation programme (Grant Agreements No. 716139 and No. 677023), the *Swiss National Science Foundation* (SNSF, PP00P2_170534, PP00P2_198900), Project PGC2018-101181-B–I00 funded by MCIN/AEI/ 10.13039/ 501100011033 FEDER "Una manera de hacer Europa", grant A-FQM-230-UGR20 funded by FEDER/Junta de Andalucía-Consejería de Transformación Económica, Industria, Conocimiento y Universidades and the German Academic Exchange Service (DAAD, postdoc fellowship to *D. G.*). Open access funding provided by the University of Zurich.

Data Availability Statement

The data that support the findings of this study are available from the corresponding author upon reasonable request.

Author Contribution Statement

D. G., *S. M.-L.*, *A. G. C.* and *M. J.* conceived the project, designed the experiments and analyzed the results. *D. G.* synthesized and characterized all compounds. *D. G.*, *S. M.-L.*, *M. J. R.-R.* and *A. O.* performed the photophysical characterization. *S. M.-L.* performed the DFT calculations. *D. G.*, *S. M.-L.*, *M. J. R.-R.*, *A. O.*, *A. G. C.* and *M. J.* co-wrote the manuscript.

 © 2022 The Authors. Helvetica Chimica Acta Published by Wiley-VHCA AG

References

[1] M. Li, S.-H. Li, D. Zhang, M. Cai, L. Duan, M.-K. Fung, C.-F. Chen, 'Stable Enantiomers Displaying Thermally Activated Delayed Fluorescence: Efficient OLEDs with Circularly Polarized Electroluminescence', *Angew. Chem. Int. Ed.* **2018**, *57*, 2889–2893.

[2] Y. Yang, R. C. da Costa, M. J. Fuchter, A. J. Campbell, 'Circularly polarized light detection by a chiral organic semiconductor transistor', *Nat. Photonics* **2013**, *7*, 634–638.

[3] Y. Yang, R. C. da Costa, D.-M. Smilgies, A. J. Campbell, M. J. Fuchter, 'Induction of Circularly Polarized Electroluminescence from an Achiral Light-Emitting Polymer via a Chiral Small-Molecule Dopant', *Adv. Mater.* **2013**, *25*, 2624–2628.

[4] G. Muller, 'Luminescent chiral lanthanide(III) complexes as potential molecular probes', *Dalton Trans.* **2009**, 9692–9707.

[5] R. Hassey, E. J. Swain, N. I. Hammer, D. Venkataraman, M. D. Barnes, 'Probing the Chiroptical Response of a Single Molecule', *Science* **2006**, *314*, 1437–1439.

[6] J. Jiménez, L. Cerdán, F. Moreno, B. L. Maroto, I. García-Moreno, J. L. Lunkley, G. Muller, S. de La Moya, 'Chiral Organic Dyes Endowed with Circularly Polarized Laser Emission', *J. Phys. Chem. C* **2017**, *121*, 5287–5292.

[7] C. M. Cruz, I. R. Márquez, S. Castro-Fernández, J. M. Cuerva, E. Maçôas, A. G. Campaña, 'A Triskelion-Shaped Saddle–Helix Hybrid Nanographene', *Angew. Chem. Int. Ed.* **2019**, *58*, 8068–8072.

[8] C. M. Cruz, S. Castro-Fernández, E. Maçôas, J. M. Cuerva, A. G. Campaña, 'Undecabenzo[7]superhelicene: A Helical Nanographene Ribbon as a Circularly Polarized Luminescence Emitter', *Angew. Chem. Int. Ed.* **2018**, *57*, 14782–14786.

[9] C. M. Cruz, I. R. Márquez, I. F. A. Mariz, V. Blanco, C. Sánchez-Sánchez, J. M. Sobrado, J. A. Martín-Gago, J. M. Cuerva, E. Maçôas, A. G. Campaña, 'Enantiopure distorted ribbon-shaped nanographene combining two-photon absorption-based upconversion and circularly polarized luminescence', *Chem. Sci.* **2018**, *9*, 3917–3924.

[10] W.-L. Zhao, M. Li, H.-Y. Lu, C.-F. Chen, 'Advances in helicene derivatives with circularly polarized luminescence', *Chem. Commun.* **2019**, *55*, 13793–13803.

[11] D.-W. Zhang, M. Li, C.-F. Chen, 'Recent advances in circularly polarized electroluminescence based on organic light-emitting diodes', *Chem. Soc. Rev.* **2020**, *49*, 1331–1343.

[12] H. Tanaka, Y. Inoue, T. Mori, 'Circularly Polarized Luminescence and Circular Dichroisms in Small Organic Molecules: Correlation between Excitation and Emission Dissymmetry Factors', *ChemPhotoChem* **2018**, *2*, 386–402.

[13] E. M. Sánchez-Carnerero, A. R. Agarrabeitia, F. Moreno, B. L. Maroto, G. Muller, M. J. Ortiz, S. de La Moya, 'Circularly Polarized Luminescence from Simple Organic Molecules', *Chem. Eur. J.* **2015**, *21*, 13488–13500.

[14] M. Rickhaus, M. Mayor, M. Juríček, 'Strain-induced helical chirality in polyaromatic systems', *Chem. Soc. Rev.* **2016**, *45*, 1542–1556.

[15] P. Ravat, R. Hinkelmann, D. Steinebrunner, A. Prescimone, I. Bodoky, M. Juríček, 'Configurational Stability of [5]Helicenes', *Org. Lett.* **2017**, *19*, 3707–3710.

[16] O. E. Weigang Jr., J. A. Turner, P. A. Trouard, 'Emission Polarization and Circular Dichroism of Hexahelicene', *J. Chem. Phys.* **1966**, *45*, 1126.

[17] K. Dhbaibi, L. Favereau, J. Crassous, 'Enantioenriched Helicenes and Helicenoids Containing Main-Group Elements (B, Si, N, P)', *Chem. Rev.* **2019**, *119*, 8846–8953.

[18] H. Sakai, S. Shinto, J. Kumar, Y. Araki, T. Sakanoue, T. Takenobu, T. Wada, T. Kawai, T. Hasobe, 'Highly Fluorescent [7]Carbohelicene Fused by Asymmetric 1,2-Dialkyl-Substituted Quinoxaline for Circularly Polarized Luminescence and Electroluminescence', *J. Phys. Chem. C* **2015**, *119*, 13937–13947.

[19] M. Sapir, E. Donckt, 'Intersystem crossing in the helicenes', *Chem. Phys. Lett.* **1975**, *36*, 108–110.

[20] H. Oyama, M. Akiyama, K. Nakano, M. Naito, K. Nobusawa, K. Nozaki, 'Synthesis and Properties of [7]Helicene-like Compounds Fused with a Fluorene Unit', *Org. Lett.* **2016**, *18*, 3654–3657.

[21] K. Dhbaibi, L. Abella, S. Meunier-Della-Gatta, T. Roisnel, N. Vanthuyne, B. Jamoussi, G. Pieters, B. Racine, E. Quesnel, J. Autschbach, J. Crassous, L. Favereau, 'Achieving high circularly polarized luminescence with push–pull helicenic systems: from rationalized design to top-emission CP-OLED applications', *Chem. Sci.* **2021**, *12*, 5522–5533.

[22] K. Dhbaibi, L. Favereau, M. Srebro-Hooper, C. Quinton, N. Vanthuyne, L. Arrico, T. Roisnel, B. Jamoussi, C. Poriel, C. Cabanetos, J. Autschbach, J. Crassous, 'Modulation of circularly polarized luminescence through excited-state symmetry breaking and interbranched exciton coupling in helical push–pull organic systems', *Chem. Sci.* **2020**, *11*, 567–576.

[23] K. Dhbaibi, P. Matozzo, L. Abella, M. Jean, N. Vanthuyne, J. Autschbach, L. Favereau, J. Crassous, 'Exciton coupling chirality in helicene-porphyrin conjugates', *Chem. Commun.* **2021**, *57*, 10743–10746.

[24] K. Dhbaibi, C. Shen, M. Jean, N. Vanthuyne, T. Roisnel, M. Górecki, B. Jamoussi, L. Favereau, J. Crassous, 'Chiral Diketopyrrolopyrrole-Helicene Polymer With Efficient Red Circularly Polarized Luminescence', *Front. Chem.* **2020**, *8*, 237.

[25] K. Dhbaibi, L. Favereau, M. Srebro-Hooper, M. Jean, N. Vanthuyne, F. Zinna, B. Jamoussi, L. Di Bari, J. Autschbach, J. Crassous, 'Exciton coupling in diketopyrrolopyrrole-helicene derivatives leads to red and near-infrared circularly polarized luminescence', *Chem. Sci.* **2018**, *9*, 735–742.

[26] A. C. Sedgwick, L. Wu, H.-H. Han, S. D. Bull, X.-P. He, T. D. James, J. L. Sessler, B. Z. Tang, H. Tian, J. Yoon, 'Excited-state intramolecular proton-transfer (ESIPT) based fluorescence sensors and imaging agents', *Chem. Soc. Rev.* **2018**, *47*, 8842–8880.

[27] V. S. Padalkar, S. Seki, 'Excited-state intramolecular proton-transfer (ESIPT)-inspired solid state emitters', *Chem. Soc. Rev.* **2016**, *45*, 169–202.

[28] J. E. Kwon, S. Y. Park, 'Advanced Organic Optoelectronic Materials: Harnessing Excited-State Intramolecular Proton Transfer (ESIPT) Process', *Adv. Mater.* **2011**, *23*, 3615–3642.

[29] P. F. Barbara, P. K. Walsh, L. E. Brus, 'Picosecond kinetic and vibrationally resolved spectroscopic studies of intramolecular excited-state hydrogen atom transfer', *J. Phys. Chem.* **1989**, *93*, 29–34.

 © 2022 The Authors. Helvetica Chimica Acta Published by Wiley-VHCA AG

[30] H.-Q. Yin, F. Yin, X.-B. Yin, 'Strong dual emission in covalent organic frameworks induced by ESIPT', *Chem. Sci.* **2019**, *10*, 11103–11109.
[31] A. Maity, F. Ali, H. Agarwalla, B. Anothumakkool, A. Das, 'Tuning of multiple luminescence outputs and white-light emission from a single gelator molecule through an ESIPT coupled AIEE process', *Chem. Commun.* **2015**, *51*, 2130–2133.
[32] K. Sakai, T. Ishikawa, T. Akutagawa, 'A blue-white-yellow color-tunable excited state intramolecular proton transfer (ESIPT) fluorophore', *J. Mater. Chem. C* **2013**, *1*, 7866–7871.
[33] D. Yao, S. Zhao, J. Guo, Z. Zhang, H. Zhang, Y. Liu, Y. Wang, 'Hydroxyphenyl-benzothiazole based full color organic emitting materials generated by facile molecular modification', *J. Mater. Chem.* **2011**, *21*, 3568–3570.
[34] C. Parthiban, M. Pavithra, L. Vinod Kumar Reddy, Dwaipayan Sen, S. Melvin Samuel, N. D. P. Singh, 'Visible-Light – Triggered Fluorescent Organic Nanoparticles for Chemo-Photodynamic Therapy with Real-Time Cellular Imaging', *ACS Appl. Nano Mater.* **2018**, *1*, 6281–6288.
[35] S. Biswas, J. Das, S. Barman, B. Rao Pinninti, T. K. Maiti, N. D. P. Singh, 'Environment Activatable Nanoprodrug: Two-Step Surveillance in the Anticancer Drug Release', *ACS Appl. Mater. Interfaces* **2017**, *9*, 28180–28184.
[36] S. Barman, S. K. Mukhopadhyay, S. Biswas, S. Nandi, M. Gangopadhyay, S. Dey, A. Anoop, N. D. Pradeep Singh, 'A *p*-Hydroxyphenacyl–Benzothiazole–Chlorambucil Conjugate as a Real-Time-Monitoring Drug-Delivery System Assisted by Excited-State Intramolecular Proton Transfer', *Angew. Chem. Int. Ed.* **2016**, *55*, 4194–4198.
[37] W.-H. Chen, Y. Xing, Y. Pang, 'A Highly Selective Pyrophosphate Sensor Based on ESIPT Turn-On in Water', *Org. Lett.* **2011**, *13*, 1362–1365.
[38] X. Yang, Y. Guo, R. M. Strongin, 'Conjugate Addition/Cyclization Sequence Enables Selective and Simultaneous Fluorescence Detection of Cysteine and Homocysteine', *Angew. Chem. Int. Ed.* **2011**, *50*, 10690–10693.
[39] R. Hu, J. Feng, D. Hu, S. Wang, S. Li, Y. Li, G. Yang, 'A Rapid Aqueous Fluoride Ion Sensor with Dual Output Modes', *Angew. Chem. Int. Ed.* **2010**, *49*, 4915–4918.
[40] W.-T. Chuang, C.-C. Hsieh, C.-H. Lai, C.-H. Lai, C.-W. Shih, K.-Y. Chen, W.-Y. Hung, Y.-H. Hsu, P.-T. Chou, 'Excited-State Intramolecular Proton Transfer Molecules Bearing *o*-Hydroxy Analogues of Green Fluorescent Protein Chromophore', *J. Org. Chem.* **2011**, *76*, 8189–8202.
[41] D. Göbel, D. Duvinage, T. Stauch, B. J. Nachtsheim, 'Nitrile-substituted 2-(oxazolinyl)-phenols: minimalistic excited-state intramolecular proton transfer (ESIPT)-based fluorophores', *J. Mater. Chem. C* **2020**, *8*, 9213–9225.
[42] D. Göbel, P. Rusch, D. Duvinage, T. Stauch, N.-C. Bigall, B. J. Nachtsheim, 'Substitution Effect on 2-(Oxazolinyl)-phenols and 1,2,5-Chalcogenadiazole-Annulated Derivatives: Emission-Color-Tunable, Minimalistic Excited-State Intramolecular Proton Transfer (ESIPT)-Based Luminophores', *J. Org. Chem.* **2021**, *86*, 14333–14355.
[43] T. R. Schulte, J. J. Holstein, G. H. Clever, 'Chiral Self-Discrimination and Guest Recognition in Helicene-Based Coordination Cages', *Angew. Chem. Int. Ed.* **2019**, *58*, 5562–5566.
[44] K. Takagi, K. Ito, Y. Yamada, T. Nakashima, R. Fukuda, M. Ehara, H. Masu, 'Synthesis and Optical Properties of Excited-State Intramolecular Proton Transfer Active π-Conjugated Benzimidazole Compounds: Influence of Structural Rigidification by Ring Fusion', *J. Org. Chem.* **2017**, *82*, 12173–12180.
[45] C.-C. Hsieh, C.-M. Jiang, P.-T. Chou, 'Recent Experimental Advances on Excited-State Intramolecular Proton Coupled Electron Transfer Reaction', *Acc. Chem. Res.* **2010**, *43*, 1364–1374.
[46] P.-T. Chou, W.-S. Yu, Y.-M. Cheng, S.-C. Pu, Y.-C. Yu, Y.-C. Lin, Huang, C.-T. Chen, 'Solvent-Polarity Tuning Excited-State Charge Coupled Proton-Transfer Reaction in *p*-*N*,*N*-Ditolylaminosalicylaldehydes', *J. Phys. Chem. A* **2004**, *108*, 6487–6498.
[47] J. Waluk, 'Hydrogen-Bonding-Induced Phenomena in Bifunctional Heteroazaaromatics', *Acc. Chem. Res.* **2003**, *36*, 832–838.
[48] T. Mori, 'Chiroptical Properties of Symmetric Double, Triple, and Multiple Helicenes', *Chem. Rev.* **2021**, *121*, 2373–2412.
[49] H. Tanaka, M. Ikenosako, Y. Kato, M. Fujiki, Y. Inoue, T. Mori, 'Symmetry-based rational design for boosting chiroptical responses', *Commun. Chem.* **2018**, *1*, 38.
[50] Gaussian 09, Revision A.02, M. J. Frisch, G. W. Trucks, H. B. Schlegel, G. E. Scuseria, M. A. Robb, J. R. Cheeseman, G. Scalmani, V. Barone, G. A. Petersson, H. Nakatsuji, X. Li, M. Caricato, A. Marenich, J. Bloino, B. G. Janesko, R. Gomperts, B. Mennucci, H. P. Hratchian, J. V. Ortiz, A. F. Izmaylov, J. L. Sonnenberg, D. Williams-Young, F. Ding, F. Lipparini, F. Egidi, J. Goings, B. Peng, A. Petrone, T. Henderson, D. Ranasinghe, V. G. Zakrzewski, J. Gao, N. Rega, G. Zheng, W. Liang, M. Hada, M. Ehara, K. Toyota, R. Fukuda, J. Hasegawa, M. Ishida, T. Nakajima, Y. Honda, O. Kitao, H. Nakai, T. Vreven, K. Throssell, J. A. Montgomery Jr., J. E. Peralta, F. Ogliaro, M. Bearpark, J. J. Heyd, E. Brothers, K. N. Kudin, V. N. Staroverov, T. Keith, R. Kobayashi, J. Normand, K. Raghavachari, A. Rendell, J. C. Burant, S. S. Iyengar, J. Tomasi, M. Cossi, J. M. Millam, M. Klene, C. Adamo, R. Cammi, J. W. Ochterski, R. L. Martin, K. Morokuma, O. Farkas, J. B. Foresman, D. J. Fox, Gaussian, Inc., Wallingford CT, 2016.
[51] Y. Liu, J. Cerezo, G. Mazzeo, N. Lin, X. Zhao, G. Longhi, S. Abbate, F. Santoro, 'Vibronic Coupling Explains the Different Shape of Electronic Circular Dichroism and of Circularly Polarized Luminescence Spectra of Hexahelicenes', *J. Chem. Theory Comput.* **2016**, *12*, 2799–2819.
[52] L. Arrico, L. Di Bari, F. Zinna, 'Quantifying the Overall Efficiency of Circularly Polarized Emitters', *Chem. Eur. J.* **2021**, *27*, 2920–2934.
[53] Y. Nagata, T. Mori, 'Irreverent Nature of Dissymmetry Factor and Quantum Yield in Circularly Polarized Luminescence of Small Organic Molecules', *Front. Chem.* **2020**, *8*, 448.
[54] Y. Nakai, T. Mori, Y. Inoue, 'Theoretical and Experimental Studies on Circular Dichroism of Carbo[*n*]helicenes', *J. Phys. Chem. A* **2012**, *116*, 7372–7385.
[55] W. L. F. Armarego, 'Purification of Laboratory Chemicals', Butterworth-Heinemann, Amsterdam, 2017.
[56] V. Církva, P. Jakubík, T. Strašák, J. Hrbáč, J. Sýkora, I. Císařová, J. Vacek, J. Žádný, J. Storch, 'Preparation and Physicochemical Properties of [6]Helicenes Fluorinated at Terminal Rings', *J. Org. Chem.* **2019**, *84*, 1980–1993.
[57] A. Granzhan, E. Largy, N. Saettel, M.-P. Teulade-Fichou, 'Macrocyclic DNA-Mismatch-Binding Ligands: Structural

 © 2022 The Authors. Helvetica Chimica Acta Published by Wiley-VHCA AG

Determinants of Selectivity', *Chem. Eur. J.* **2010**, *16*, 878–889.

[58] M. Linseis, S. Záliš, M. Zabel, R. F. Winter, 'Ruthenium Stilbenyl and Diruthenium Distyrylethene Complexes: Aspects of Electron Delocalization and Electrocatalyzed Isomerization of the *Z*-Isomer', *J. Am. Chem. Soc.* **2012**, *134*, 16671–16692.

[59] P. N. Chalikidi, T. T. Magkoev, A. V. Gutnov, O. P. Demidov, M. G. Uchuskin, I. V. Trushkov, V. T. Abaev, 'One-Step Synthesis of Triphenylphosphonium Salts from (Het)arylmethyl Alcohols', *J. Org. Chem.* **2021**, *86*, 9838–9846.

[60] M. T. Reetz, E. W. Beuttenmüller, R. Goddard, 'First enantioselective catalysis using a helical diphosphane', *Tetrahedron Lett.* **1997**, *38*, 3211–3214.

[61] A. Terfort, H. Görls, H. Brunner, 'The First Helical-Chiral Phosphane Ligands: *rac*-[5]- and *rac*-[6]-Heliphos', *Synthesis* **1997**, 79–86.

[62] T. Ishiyama, M. Murata, N. Miyaura, 'Palladium(0)-Catalyzed Cross-Coupling Reaction of Alkoxydiboron with Haloarenes: A Direct Procedure for Arylboronic Esters', *J. Org. Chem.* **1995**, *60*, 7508–7510.

[63] D. Göbel, N. Clamor, E. Lork, B. J. Nachtsheim, 'Aerobic C(sp^2)–H Hydroxylations of 2-Aryloxazolines: Fast Access to Excited-State Intramolecular Proton Transfer (ESIPT)-Based Luminophores', *Org. Lett.* **2019**, *21*, 5373–5377.

[64] J. Malinčík, S. Gaikwad, M.-A. Boillat, D. Häussinger, T. Solomek, 'Figure-of-Eight Helicene Carbon Nanohoop with Möbius Topology', *ChemRxiv.* **2021**; https://doi.org/10.26434/chemrxiv.13817498.v1.

Received October 21, 2021
Accepted February 17, 2022